Electronic Supplementary Information

d_{z^2} Orbital character of polyhedra in complex solid-state transition-metal compounds

Isao Ohkubo*[a,b,c] and Takao Mori[a,b]

[a]Center for Functional Sensor & Actuator (CFSN), Research Center for Functional Materials, National Institute for Materials Science (NIMS), 1-1 Namiki, Tsukuba, Ibaraki 305-0044, Japan

[b]International Center for Materials Nanoarchitectonics (MANA), National Institute for Materials Science (NIMS), 1-1 Namiki, Tsukuba, Ibaraki 305-0044, Japan

[c]Center for Materials Research by Information Integration (CMI^2), Research and Services Division of Materials Data and Integrated System (MaDIS), National Institute for Materials Science (NIMS), 1-1 Namiki, Tsukuba, Ibaraki 305-0044, Japan

*Corresponding author, e-mail address: OHKUBO.Isao@nims.go.jp

Contents **Page**

List of Figures

1. Description of calculations

The electronic-structure calculations were performed by using the L/APW+lo method, as implemented in the WIEN2k code.[S1] The generalized gradient approximation-PerdewŬBurkeŬErnzerhof functional (GGA-PBE) [S2,S3] and the modified BeckeŬJohnson exchange potential (mBJ) were used.[S4,S5] A GGA-PBE+U approach was also adopted, where U is the effective on-site Coulomb interaction correction. All calculations were performed by using experimental structural coordinates and lattice constants taken from powder neutron and X-ray diffraction measurements. The 4H-type hexagonal perovskite $BaTiO_3$ crystallizes with a *P6₃/mmc* structure (space group No. 194) with Ba atoms situated at the (0, 0, 1/4) and the (1/3, 2/3, 0.096715) sites, Ti atoms at the (0, 0, 0) and the (1/3, 2/3, 0.8463314) sites, and O atoms at the (0.51856, 0.0370, 1/4) and the (0.83496, 0.6698, 0.08022) sites.[S6] The lattice parameters are $a = 5.72387$ Å and $c = 13.96497$ Å. The 2H-type hexagonal perovskites $BaTiS_3$ and $SrTiS_3$ also crystallize with a $P6_3/mmc$ structure (space group No. 194), with Ba (Sr) atoms situated at the (1/3, 2/3, 1/4) site, Ti atoms at the (0, 0, 0) site, and S at the (0.16551, 0.33212, 1/4) site for $BaTiS_3$ or the (0.166, 0.332, 1/4) site for $SrTiS_3$.[S7,S8] The lattice constants are a#= 6.756 Å, $c = 5.798$ Å for $BaTiS_3$ and $a = 6.59$ Å, $c = 5.708$ Å for $SrTiS_3$.

To calculate the electronic structures of α-$NaFeO_2$-type $SrMN_2$ (M = Zr, Hf) and $LiMoN_2$ by using the WIEN2k code, the lattice constants of the hexagonal system and the atomic positions of the rhombohedral system were used. α-$NaFeO_2$-type $SrMN_2$ (M = Zr, Hf) crystallizes in the *R-3m* structure (space group No. 166), with the Sr atoms situated at the (1/2, 1/2, 1/2) site, M-type atoms at the (0, 0, 0) site, and N at the (z, z, z) site ($z = 0.23502$ for $SrZrN_2$, $z = 0.23463$ for $SrHfN_2$).[S9] The hexagonal lattice constants for these calculations are $a = 3.373$ Å, $c = 17.676$ Å for $SrZrN_2$, and $a = 3.345$ Å, $c = 17.678$ Å for $SrHfN_2$. $LiMoN_2$ crystallizes in the *R3* structure (space group No. 146), with the Li atoms situated at the (0.829018, 0.829018, 0.829018) site, Mo atoms at the (0, 0, 0) site, and N at the (0.25204, 0.25204, 0.25204) site and the (0.41414, 0.41414, 0.41414) site.[S10] The lattice constants are $a = 2.86723$ Å, $c = 15.813$ Å. $LiWN_2$ crystallizes in the $P6_3/mmc$ structure (space group No. 194), with the Li atoms situated at the (0, 0, 0) site, W atoms at the (1/3, 2/3, 1/4) site, and N at the (1/3, 2/3, 0.65253) site.[S11] The lattice constants are a#= 2.881 Å, $c = 10.346$ Å. The parameter $R_{mt}K_{max}$, where R_{mt} is the smallest muffin-tin radius (in atomic units) and K_{max} is the plane wave cutoff, controls the size of the basis, which was set to a high value of 7.0 for all materials. The values of R_{mt} for the atomic spheres were 2.5 (Ba), 1.93 (Ti), 1.75 (O) for 4H-$BaTiO_3$; 2.5 (Ba), 2.45 (Ti), 2.11 (S) for 2H-$BaTiS_3$; 2.5 (Sr), 2.39 (Ti), 2.06 (S) for 2H-$SrTiS_3$; 2.26 (Sr), 2.08 (Zr), 1.79 (N) for $SrZrN_2$; 2.25 (Sr), 2.11 (Hf), 1.73 (N) for $SrHfN_2$; 1.82 (Li), 2.11 (Mo), 1.82 (N) for $LiMoN_2$; and 1.83 (Li), 2.17 (W), 1.78 (N) for $LiWN_2$. 100 ***k***-points in the Brillouin zones were used in calculating the electronic structures. The Brillouin zones for the electronic band structures of 4H-type hexagonal perovskite $BaTiO_3$, 2H-type hexagonal perovskite $BaTiS_3$, 2H-$SrTiS_3$, $LiWN_2$, and $LiMoN_2$ are shown in Figure S1.

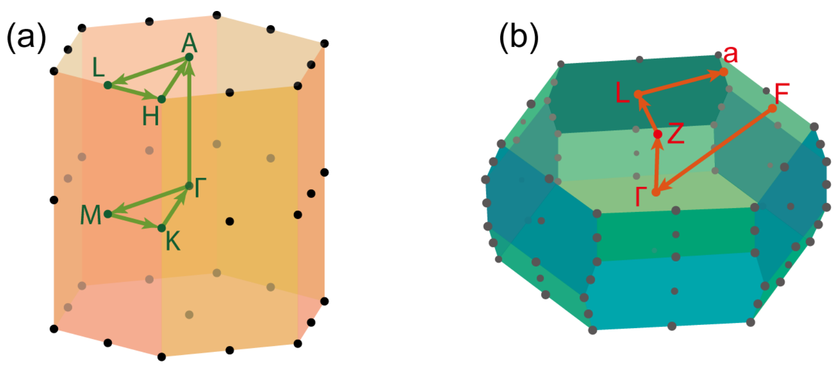

Figure S1. Brillouin zones for the electronic band structures of (a) 4H-type hexagonal perovskite $BaTiO_3$, 2H-type hexagonal perovskite $BaTiS_3$, 2H-$SrTiS_3$, and $LiWN_2$ and (b) of $LiMoN_2$.

2. Electronic structure of 2H-type hexagonal perovskite $SrTiS_3$ composed of face-sharing octahedra

Figure S2 shows the electronic band structure and the orbital characters for the lowest conduction band of the 2H-type hexagonal perovskite $SrTiS_3$, which consists of face-sharing TiS_6 octahedral blocks. The results of electronic calculations for 2H-$SrTiS_3$ using the GGA-PBE functional and the mBJ exchange potential do not show energy-band gaps if the on-site Coulomb interaction is not considered. Energy-band gaps in 2H-$SrTiS_3$ are observed in the electronic structures calculated by the GGA-PBE+U method if the effective Coulombic interaction $U_{\mathrm{eff}} > 8$ eV: an effective on-site U_{eff} was therefore taken into account for the Ti site. The calculated energy-band gap (direct) of 2H-$SrTiS_3$ at the Γ-point is 0.18 eV ($U_{\mathrm{eff}} = 9$ eV). The energy-band gaps vary depending on the value of U_{eff}. Figure S3 shows the density of states (DOS) in 2H-$SrTiS_3$. The lowest conduction band and the highest valence band in 2H-$SrTiS_3$ have mainly Ti 3d and S 3p orbital characters, respectively. Orbital characters for the lowest conduction band are shown in Figures S2b. Ti 3d_{z^2} (a_{1g}) orbital character predominates in the lowest conduction band, except for the LŨH directions. In the L–H directions of the electronic band structures, the Ti 3$d_{x^2-y^2}$ + 3d_{xy} orbitals are dominant.

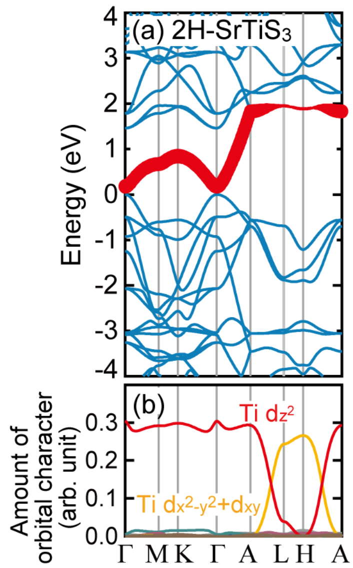

Figure S2. (a) Electronic band structure and (b) orbital characters for the lowest conduction band in the 2H-hexagonal perovskite $SrTiS_3$. The amount of Ti 3d_{z^2} orbital character is shown by the width of the lines in the lowest conduction band. In Figure S2b, all s orbitals, p orbitals (p_z, $p_x + p_y$ for Sr and Ti, p_x, p_y, p_z for S), and d orbitals (d_{z^2}, $d_{x^2-y^2} + d_{xy}$, $d_{xz} + d_{yz}$ for Sr and Ti) are plotted. The electronic band structure was calculated by the GGA-PBE+U method ($U_{\mathrm{eff}} = 9$ eV).

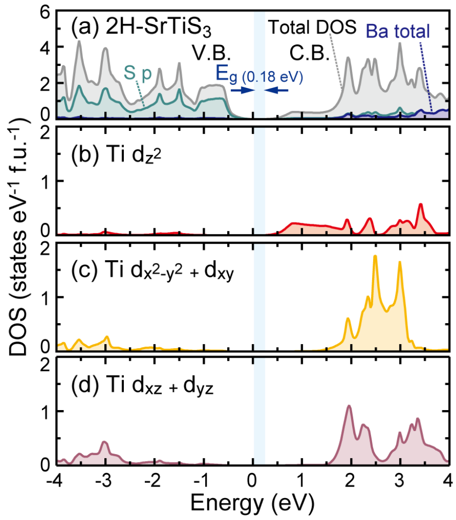

Figure S3. Total and partial density of states (DOS) of d orbitals in the 2H-hexagonal perovskite $SrTiS_3$. (a) Total DOS and partial DOS of Sr and S 3p orbitals, (b) d_{z^2}, (c) $d_{x^2-y^2} + d_{xy}$, (d) $d_{xz} + d_{yz}$ orbitals. The DOSs were calculated by the GGA-PBE+U method (U_{eff} = 9 eV).

3. Electronic structure of α-$NaFeO_2$-type $SrHfN_2$ consisting of edge-sharing octahedral layers

Figure S4 shows the density of states (DOS) in the α-$NaFeO_2$-type d^0-layered complex metal nitride $SrHfN_2$, which consists of edge-sharing HfN_6 octahedral layers. The DOSs of $SrHfN_2$ were calculated by using the mBJ exchange potential. The main contributors to the valence bands and the conduction bands are N 2p orbitals and Hf 5d orbitals, respectively. As with the other α-$NaFeO_2$-type d^0-layered complex metal nitrides $SrZrN_2$, $NaNbN_2$, and $NaTaN_2$, the Hf $5d_{z^2}$ orbital characters predominate at the bottom of the conduction band (F-point).[S12,S13]

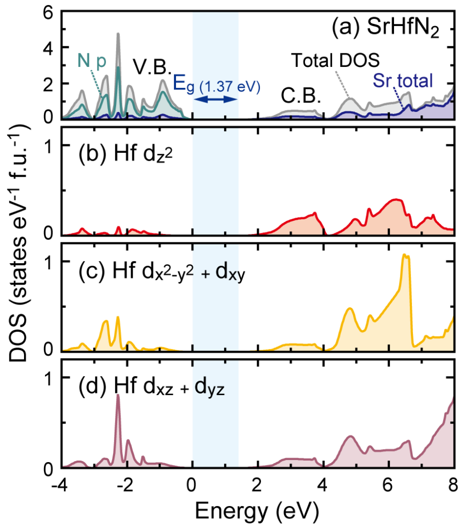

Figure S4. Total and partial density of states (DOS) of d orbitals in α-$NaFeO_2$-type $SrHfN_2$. (a) Total DOS and partial DOS of Sr and N 2p orbitals, (b) d_{z^2}, (c) $d_{x^2-y^2} + d_{xy}$, (d) $d_{xz} + d_{yz}$ orbitals. These DOSs were calculated by using the mBJ exchange potential.

4. Electronic structure of $LiWN_2$ consisting of edge-sharing trigonal prismatic layers

The electronic band structure and the orbital characters for the lowest conduction band in $LiWN_2$ are shown in Figure S5. Electronic structures of $LiWN_2$ were calculated by using the GGA-PBE functional. In $LiWN_2$, three electronic bands (Bands C, D, and E) cross the Fermi level (0 eV). In Bands C and D, the predominant orbital characters are W $5d_{x^2-y^2}$ + $5d_{xy}$ near the Fermi level and near the K- and H-points, and W $5d_{z^2}$ below the Fermi level and near the Γ- and A-points. In Band E, N 2p orbital character predominates. In Bands A and B, the dominant orbital characters are W $5d_{z^2}$ near the K- and H-points, and W $5d_{x^2-y^2}$ + $5d_{xy}$ in the Γ–A direction and near the K-point. As shown in Figure S6, large contributions from W $5d_{z^2}$ and $5d_{x^2-y^2}$ + $5d_{xy}$ orbitals are separately present near the Fermi level (0 eV) and at about 4 eV, corresponding to locations of Bands C and D near the Fermi level and of Bands A and B at about 5 eV. The electronic structure also contains some N 2p orbital character near the Fermi level and at about 4 eV (Figure S6). Hybridized orbital characters combining W $5d_{z^2}$, $5d_{x^2-y^2}$ + $5d_{xy}$ with N 2p are present in the electronic bands near the Fermi level (0 eV) and at about 4 eV.

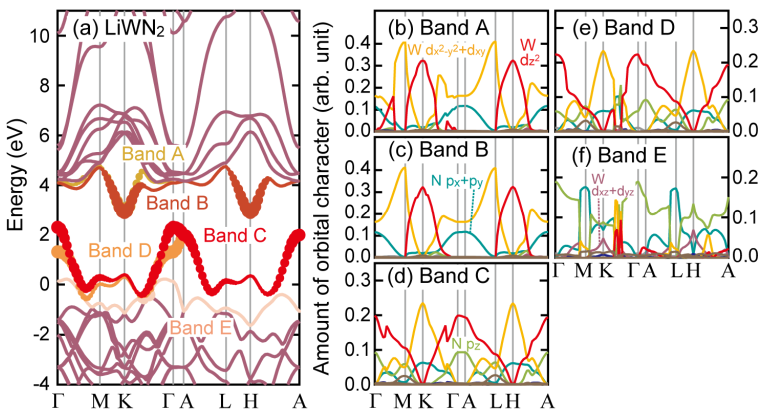

Figure S5. (a) Electronic band structure and (b–f) orbital characters of electronic bands (Bands A–E) near the Fermi level in $LiWN_2$. The amounts of W $5d_{z^2}$ orbital characters are shown in the electronic band structures by the widths of the line (Bands A–E near the Fermi level). All s orbitals, p orbitals (p_z, $p_x + p_y$ for W, p_x, p_y, p_z for N), and d orbitals (d_{z^2}, $d_{x^2-y^2} + d_{xy}$, $d_{xz} + d_{yz}$ for W) are plotted in Figures S5b–S5f. The electronic band structure was calculated by using the GGA-PBE functional.

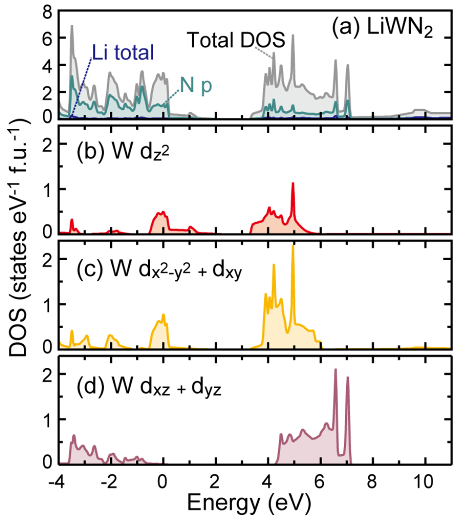

Figure S6. Total and partial density of states (DOS) of d orbitals in $LiWN_2$. (a) Total DOS and partial DOS of Li and N 2p orbitals, (b) d_{z^2}, (c) $d_{x^2-y^2} + d_{xy}$, (d) $d_{xz} + d_{yz}$. The DOSs were calculated by using the GGA-PBE functional.

5. Supplementary references

(S1) P. Blaha, K. Schwarz, G. Madsen, D. Kvasicka, and J. Luitz, *Wien2k: An Augmented Plane Wave Plus Local Orbitals Program for Calculating Crystal Properties*; TU Vienna: Vienna, Austria, 2001.

(S2) J. P. Perdew, K. Burke, and M. Ernzerhof, *Phys. Rev. Lett.* 1996, **77**, 3865–3868.

(S3) J. P. Perdew, K. Burke, and M. Ernzerhof, *Phys. Rev. Lett.* 1997, **78**, 1396.

(S4) F. Tran, P. Blaha, *Phys. Rev. Lett.* 2009, **102**, 226401.

(S5) D. Koller, F. Tran, and P. Blaha, *Phys. Rev. B: Condens. Matter,* 2011, **83**, 195134.

(S6) J. Akimoto, Y. Gotoh, and Y. Oosawa, *Acta Cryst.* 1994, **C50**, 160–161.

(S7) J. Huster, *Z. Naturforsch. B,* 1980, **35**, 775.

(S8) H. Hahn, U. Mutschke, *Z. Anorg. Allg. Chem.* 1956, **288**, 269–278.

(S9) D. H. Gregory, M. G. Barker, P. P. Edwards, D. J. Siddons, *Inorg. Chem.* 1996, **35**, 7608–7613.

(S10) S. H. Elder, L. H. Doerrer, F. J. DiSalvo, J. B. Parise, D. Guyomard, and J. M. Tarascon, *Chem. Mater.* 1992, **4**, 929–937.

(S11) S. Kaskel, D. Hohlwein, and J. Strähle, *J. Solid State Chem.* 1998, **138**, 154–159.

(S12) I. Ohkubo and T. Mori, *Inorg. Chem.* 2014, **53**, 8979–8984.

(S13) I. Ohkubo and T. Mori, *APL Mater.* 2016, **4**, 104808.